New Journal of Physics
The open-access journal for physics

Solitary localized structures in a liquid crystal light-valve experiment

U Bortolozzo[1], M G Clerc[2,3] and S Residori[1]

[1] INLN, Université de Nice Sophia-Antipolis, CNRS, 1361 route des Lucioles, 06560 Valbonne, France

[2] Departamento de Física, Facultad de Ciencias Físcas y Matemática, Universidad de Chile, Casilla 487-3, Santiago, Chile

E-mail: ubortolozzo@yahoo.com, marcel@dfi.uchile.cl and stefania.residori@inln.cnrs.fr

New Journal of Physics **11** (2009) 093037 (10pp)
Received 18 January 2009
Published 28 September 2009
Online at http://www.njp.org/
doi:10.1088/1367-2630/11/9/093037

Abstract. In a liquid crystal light-valve experiment, we report solitary localized structures appearing outside the bistability range and displaying a behavior of single independent cells. The transition from an extended pattern to solitary states is characterized both experimentally and numerically.

Contents

[3] Author to whom any correspondence should be addressed.

1. Introduction

The concept of *soliton* as a single coherent structure originates from Hamiltonian systems [1]. The generalization of this concept to dissipative and out of equilibrium systems has led to several studies in the last few decades, in particular to the definition of *localized structures* intended as patterns appearing in a restricted region of space ([2] and reference therein). Localized structures have been observed in different fields, such as magnetic materials [3], granular media [4, 5], vibrated fluids [6], electroconvection [7], plasmas [8], chemical reactions [9], nonlinear optical systems [10, 11], semiconductor microcavities [12], atomic vapors [13] and liquid crystals [14].

All these observations have inspired many theoretical works on the origin of localized structures. Most of them are based on a one-dimensional geometrical description, in which localized structures are understood as the homoclinic orbits in the Poincaré section of the corresponding spatial-reversible dynamical system [15]–[17]. In this framework, localized structures are predicted to exist in parameter regions where the system exhibits bistability between two stable spatial states and are understood as macroscopic particle-like objects realizing the spatial connection between the two metastable states and appearing close to the *pinning range* of the front solution [18]. Inside the pinning range, the bifurcation diagram displays a *snaking* shape with an infinite sequence of saddle-node bifurcations, each bifurcation creating a cell of the localized pattern solution [16]. Extensions of the same scenario have been given in later papers [19]–[21]. More recently, localized structures have been described in terms of front interactions [22] and their existence has been generalized to the case when the homoclinic orbits connect two pattern states, thus leading to *localized peaks* [23].

Despite the intuitive picture given by the geometrical approaches, the comparison with the experiments remains hard to establish, the main discrepancy originating from the large robustness of the one-cell localized structures, which we will call *solitary localized structures* (SLS), with respect to the other solutions predicted by the infinite sequence of homoclinic orbits inside the snaking region. Indeed, several observations in optics [12]–[14], vibrated granular media [4] or electroconvection [7] indicate that localized structures display more a character of single objects than that of differently sized patterns, that is, only the single-cell localized structures appear. Moreover, solitary structures often appear outside the range of bistability between the homogeneous and the pattern state, which is also confirmed by numerical simulations, for example on cavity solitons [24].

The theory–experiment discrepancy has been recently addressed and a solution is proposed, which is based on the inclusion of non-local terms in the modified Swift–Hohenberg equation [25] and leads to a tilt of the snaking bifurcation diagram [26]. Another approach relies on the development of a local theory, showing that a slanted homoclinic snaking can in general result from a saddle-node bifurcation of the pattern solution exhibited by a non-resonant amplitude equation [27]. Recently, the existence of localized solutions outside the bistability region, and associated tilted snaking diagrams, have been proved rigourously for two-dimensional Swift–Hohenberg equation [28].

In this paper, we show, both experimentally and numerically, that SLS (one-cell) exist outside the bistability range and that the transition from the extended pattern to solitary states takes place through a mechanism of particle collision and annihilation, at difference with the front propagation predicted to occur at the boundaries of the pinning region. We support our observations by characterizing the evolution of the probability density functions (PDFs) of the

light intensity fluctuations for a liquid crystal light valve (LCLV) with optical feedback. We confirm the results by numerical simulations of a full model derived from first principles.

2. Description of the experiment and derivation of the model from first principles

The experiment consists of an LCLV inserted in an optical feedback loop [29]. The LCLV is composed of a nematic liquid crystal layer in between a glass wall and a photoconductive plate over which a dielectric mirror is deposed. The liquid crystals are planar aligned (nematic director parallel to the confining walls) and the thickness of the layer is 15 μm. Transparent electrodes covering the cell walls permit the application of an external voltage V_0. The photoconductor behaves like a variable impedance, its resistance decreasing when the intensity is increased. When a voltage V_0 is applied to the valve, the voltage that effectively drops across the liquid crystals is $V_{\mathrm{LC}} = \Gamma V_0 + \alpha I_{\mathrm{w}}$, where I_{w} is the light intensity impinging on the photoconductor side of the LCLV and Γ, α are phenomenological parameters summarizing, in the linear approximation, the response of the photoconductor. The input beam, when passing through the liquid crystal layer, undergoes a phase shift $\varphi = \beta \cos^2\theta$, with θ the average tilt angle of the liquid crystal molecules and $\beta = 2\pi\Delta n d/\lambda$, where λ is the optical wavelength and $\Delta n = n_{\mathrm{e}} - n_0$ is the liquid crystal birefringence, n_{e} and n_0 being, respectively, the extraordinary (parallel to the liquid crystal director $\vec{n}$) and ordinary (perpendicular to $\vec{n}$) refractive index. The tilt angle θ obeys a diffusion relaxation equation [30],

$$\tau \partial_t \theta = l^2 \nabla_\perp^2 \theta - \theta + f(\theta), \tag{1}$$

where $l = 20\,\mu$m is the diffusion length summarizing the elastic coupling in the liquid crystal and the charge diffusion in the photoconductor, $\tau = 10$ ms is the local relaxation time, $f(\theta) = \pi/2(1 - \sqrt{V_{\mathrm{FT}}/V_{\mathrm{LC}}})$ accounts for the response of the LCLV and $V_{\mathrm{FT}} = 1.05$ V is the Fréedericksz transition voltage [31]. The optical feedback is obtained by sending back onto the photoconductor the light that has passed through the liquid crystals and has been reflected by the LCLV. After free propagation and polarization interference, the light intensity arriving at the photoconductor is

$$I_{\mathrm{w}} = \frac{I_{\mathrm{in}}}{4} \mid \mathrm{e}^{\mathrm{i}(L\lambda/4\pi)\nabla_\perp^2} \cdot (1 - \mathrm{e}^{\mathrm{i}\beta\cos^2\theta}) \mid^2, \tag{2}$$

where I_{in} is the input intensity and L is the free propagation length in the optical feedback loop. equations (1) and (2) constitute the full model equations for our system.

3. Characterization of the transition from an extended pattern to SLS

In the experiment, we fix the free propagation length to $L = 8$ cm. As control parameters, we change the applied voltage V_0 and the input light intensity I_{in}. By varying either V_0 or I_{in} we observe different dynamical regimes. The transition from an extended hexagonal (HEX) pattern to SLS occurs in a wide range of the V_0, I_{in} parameters. This type of transition has been studied in the framework of passive diffractive resonator [32]. Figure 1 shows the region of existence of SLS in $V_0 - I_{\mathrm{in}}$ plane. Dots are experimental points obtained by detecting the pattern change when varying the voltage V_0 for each value of the input intensity I_{in}.

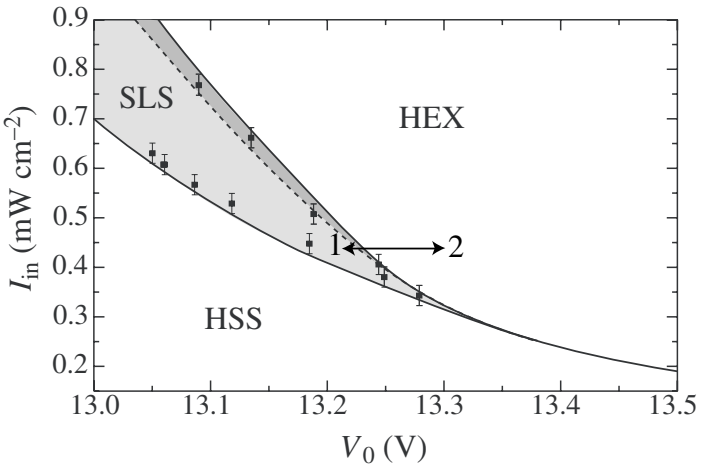

Figure 1. Phase diagram in the $I_{in} - V_0$ plane of the LCLV experiment. Lines are numerically calculated, dots are the experimental points. The dashed line delimits the region of bistability between the homogeneous steady state (HSS) and the pattern (HEX) state.

Curves in figure 1 are numerically calculated from the model equations (1) and (2) by fixing the parameters in the region of existence of SLS and then switching on a single localized structure by a triggering pulse. The voltage is increased until the transition toward hexagons occurs, or is decreased until the HSS is reached. The same procedure is repeated starting from the extended pattern and by decreasing the voltage until the homogeneous solution is approached. The continuous lines mark the boundaries of the region of existence of SLS. The dashed line delimits the region of bistability between the HSS and the HEX state. This region is very narrow and in the experiment is masked by the liquid crystal inhomogeneities. Note also that for input intensity $I_{in} \geqslant 0.8\,\mathrm{mW\,cm^{-2}}$ a transition from hexagons to space-time chaos occurs and for voltage $V_0 \leqslant 13.05\,\mathrm{V}$ we observe the formation of triangular localized structures [33]. In this case the transition to extended pattern shows a more complex scenario [34], that will not be discussed here.

Experimentally, the boundary between HSS and SLS is found by applying a local perturbation at the HSS state and by checking if one or more solitary structures remain after removing the perturbation. On the other side, the boundary between the HEX and the SLS is determined by starting with V_0 in the HEX region and then decreasing it to the SLS region. We show in figure 2 three typical instantaneous snapshots recorded for $I_{in} = 0.38\,\mathrm{mW\,cm^{-2}}$ and by changing the rms value of V_0 from 13.30 to 13.22 V. We first observe an hexagonal pattern (figure 2(a)). When decreasing the voltage, a transition takes place and the system evolves toward a final distribution of SLS appearing in random space positions (figure 2(c)). During the transition, the solitary structures interact with each other (figure 2(b)), displaying a gas-like behavior characterized by continuous collisions between the particles. At difference with a real gas, the collisions may lead to particle annihilation, so that in the course of time the number of particles is not conserved.

After a transient, which lasts for a few seconds, a final frozen configuration of SLS is reached, where the particles remain fixed in their position and interactions become negligible. Starting from different initial conditions, different final frozen configurations are observed,

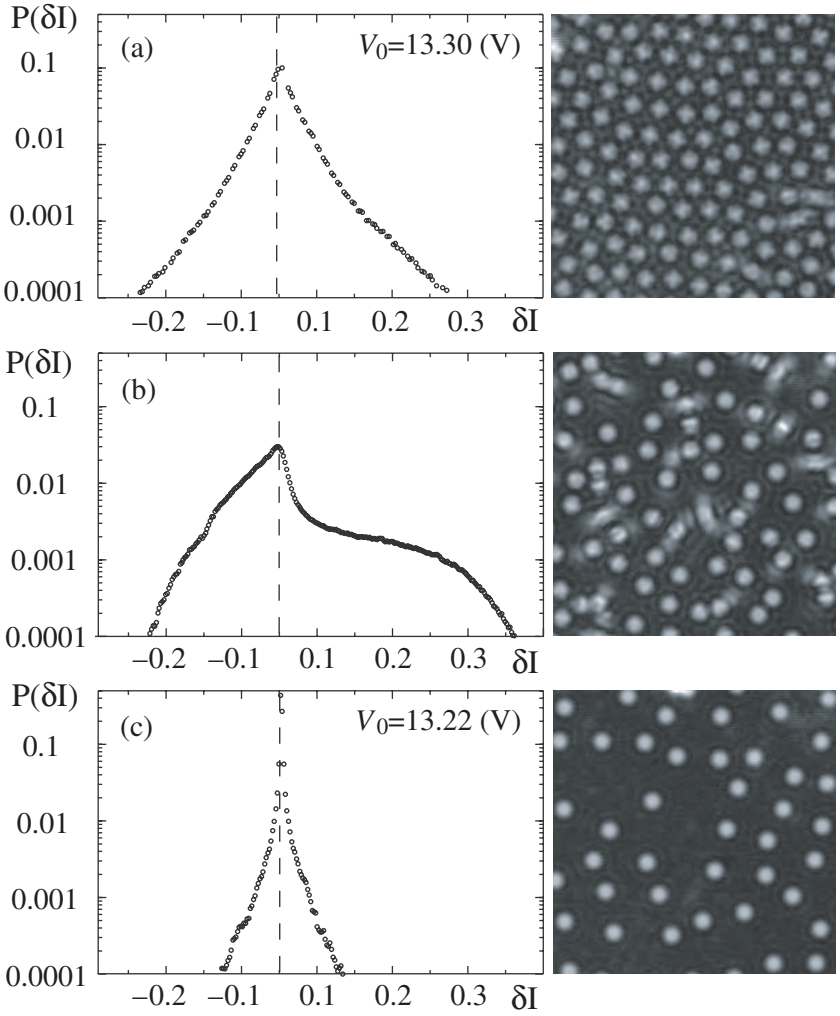

Figure 2. Experimental PDF (left) and instantaneous snapshots (right) showing the transition from (a) a HEX pattern to (c) a frozen configuration of SLS, through (b) a transient characterized by particle interaction and annihilation.

so that we can identify the state of figure 2(c) as one with a large configurational entropy, in the sense defined in [35]. Note that SLS always remain individuals and do not form a pattern, as can be remarked by the empty space between them. We can also note in figure 2(b) (at difference with figure 2(a)) the presence of oscillatory rings around each individual cell, these rings being due to the diffraction of a single spot over the uniform background and being absent in a pattern, or in a patch of pattern as it would result if the transition would occur through the propagation of a front expanding from differently sized localized patterns.

In order to characterize the observed dynamical states, we have recorded long-time movies and from each movie we have extracted the PDF of the light intensity fluctuations $\delta I = I - \langle I \rangle$, where I is the intensity of each pixel and $\langle I \rangle$ is the average intensity distribution, which is calculated by averaging pixel by pixel over the entire stack of images. The results are shown in the left part of figure 2. The HEX state and the frozen configuration of SLS are almost

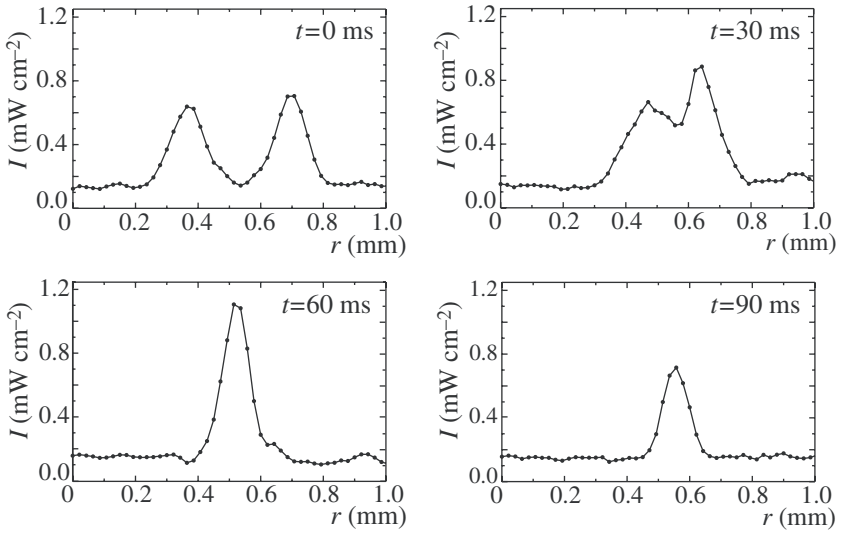

Figure 3. Experimental profiles recorded during a two-particle collision.

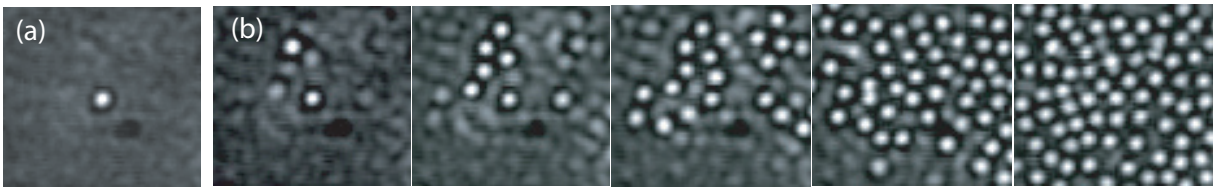

Figure 4. Experimental snapshots showing the transition from the SLS (state 1) to the HEX pattern (state 2); (a) $V_0 = 13.22\,\mathrm{V}$, (b) $V_0 = 13.30\,\mathrm{V}$: successive frames correspond to successive instant times with a time step of 0.4 s; $I_{\mathrm{in}} = 0.45\,\mathrm{mW\,cm^{-2}}$. An animation of this figure is available from stacks.iop.org/NJP/11/093037/mmedia.

stationary states and the PDFs are given by fluctuations of the particles around their equilibrium positions. In the HEX state, the PDF is larger because of slow sliding and gliding of differently oriented domains, whereas for the frozen gas only the fluctuations due to inhomogeneities and noise naturally present in the system are influencing the stationary state. The transition from hexagons to solitary structures is characterized by an abrupt change of the PDF that becomes strongly asymmetric acquiring a high tail at large intensity fluctuations (figure 2(b)). These large fluctuations correspond to events of particle annihilations, when high intensity pulses are produced during the collisions of two particles.

In figure 3 is displayed a set of experimental profiles recorded during an event of two-particle collision. It can be seen that a high intensity pulse is produced when the two particles collide and that after the collision one particle has been annihilated.

On the other side, the transition from the SLS (state 1) to the HEX pattern (state 2) occurs by starting with V_0 in the SLS region and then increasing it to the HEX region. Experimentally, a single localized structure is created in the SLS state by applying a local, and small, perturbation. In figure 4, we show a set of experimental snapshots recorded during the transition from a single localized structure to an hexagonal pattern. The input intensity is

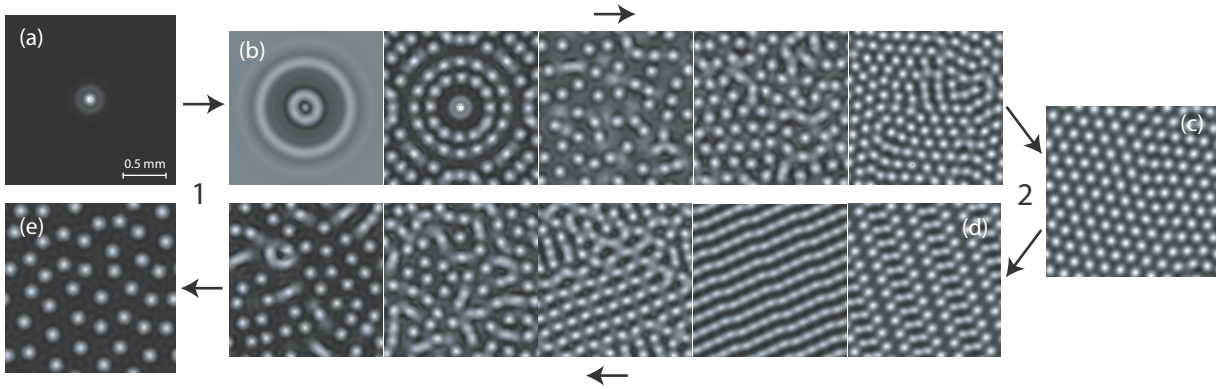

Figure 5. Numerical snapshots showing the evolution of the liquid crystal tilt angle $\theta(x, y, t)$ during the transition $1 \rightarrow 2 \rightarrow 1$. The spatial scales are identical in all panels. (a) $V_0 = 13.22\,\mathrm{V}$ with a single localized structure (state 1); (b) $V_0 = 13.22\,\mathrm{V}$: successive frames correspond to successive instant times with a time step of 0.4 s; $I_{\mathrm{in}} = 0.45\,\mathrm{mW\,cm^{-2}}$; (c) final HEX pattern (state 2); (d) $V_0 = 13.22\,\mathrm{V}$: successive frames correspond to successive instant times with a time step of 0.4 s; (e) final state of SLS (state 1). An animation of this figure is available from stacks.iop.org/NJP/11/093037/mmedia.

$I_{\mathrm{in}} = 0.45\,\mathrm{mW\,cm^{-2}}$ and the voltage is first fixed to $V_0 = 13.22\,\mathrm{V}$, panel (a). Then, it is increased to $V_0 = 13.30\,\mathrm{V}$, panel (b). The successive frames on the same line correspond to successive instant times with a time step of 0.4 s. We can see that the evolution toward the HEX state takes place through the nucleation of new cells in random space positions, triggered mainly by the spatial inhomogeneities of the liquid crystal orientation.

4. Numerical simulations

Numerical simulations of the full model for the LCLV system—equations (1) and (2)—are performed by a pseudo-spectral method and Runge–Kutta integration and by fixing periodic boundary conditions. In order to characterize the transition $1 \rightarrow 2 \rightarrow 1$, as marked in figure 1, we have performed simulations for either increasing or decreasing the control parameter V_0 and by keeping fixed the input intensity at $I_{\mathrm{in}} = 0.45\,\mathrm{mW\,cm^{-2}}$.

In figure 5, we show the transitions $1 \rightarrow 2 \rightarrow 1$. In panel (a) the voltage is fixed to $V_0 = 13.22\,\mathrm{V}$ and a single localized structure is switched on by a triggering intensity pulse (state 1). Then, the voltage is increased to $V_0 = 13.22\,\mathrm{V}$, panel (b). The successive frames on the same line show the evolution toward the final HEX state, panel (c). In panel (d) the voltage is decreased back to its initial value, $V_0 = 13.22\,\mathrm{V}$, and the successive frames on the same line show the evolution toward the final SLS state, panel (e).

Both from the top and the bottom line of the temporal evolution (direct, respectively, reverse transition from SLS to HEX), we note that the intermediate states are characterized by a process of filamentation and successive break-up, which can lead either to cells replication or annihilation. Note that a similar mechanisms of spot self-replication has recently been described for a Schnakenburg model in a two-dimensional domain [36] and for the spot deformation and replication in the two-dimensional Belousov–Zhabotinski reaction–diffusion system [37].

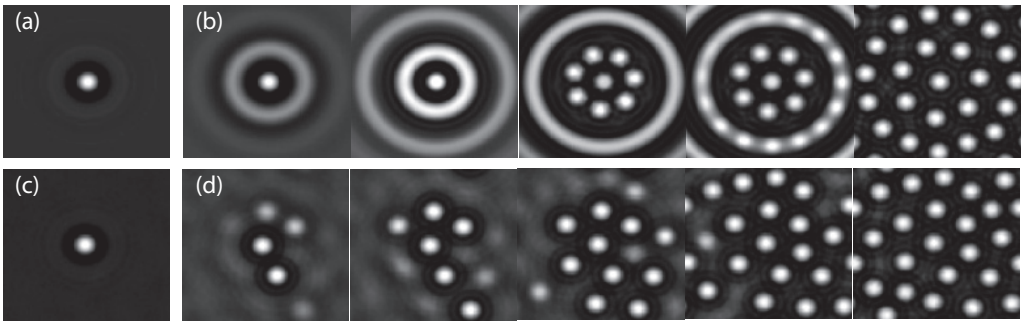

Figure 6. Numerical snapshots showing the evolution of the liquid crystal tilt angle $\theta(x, y, t)$ during the transition from the SLS (state 1) to the HEX pattern (state 2); (a) and (c) $V_0 = 13.22\,\mathrm{V}$, (b) and (d) $V_0 = 13.30\,\mathrm{V}$: on each line successive frames correspond to successive instant times with a time step of 0.4 s; $I_{\mathrm{in}} = 0.45\,\mathrm{mW\,cm^{-2}}$. The top line shows the evolution in the absence of noise, the bottom line shows the evolution in the presence of a spatial noise distribution with an amplitude less than 4% of the maximum pattern amplitude.

The numerical transition from HEX to SLS displays the same scenario as the one observed in the experiment, with a transient characterized by particle interactions, collisions and annihilations. Correspondingly, the PDF of the intensity obtained from the numerical simulations are in good agreement with the experimental PDFs. As for the SLS to HEX transition we observe that new cells nucleate spontaneously over concentric rings around the first cell, while in the experiment this behavior is not observed and localized structures nucleate instead in random space positions. This different behavior is due to the presence of spatial inhomogeneities that destroy the radial symmetry of the ring-shaped disturbances around the first localized structure.

To test the influence of spatial inhomogeneities, we have performed numerical simulations of the $1 \rightarrow 2$ transitions by adding a small amplitude distribution of spatial noise. The maximum noise amplitude is kept less than 4% of the maximum pattern amplitude. In figure 6, we show the first stages of the transition $1 \rightarrow 2$ with and without noise. The top and bottom lines display numerical snapshots of the liquid crystal tilt angle $\theta(x, y, t)$ with and without noise, respectively. In figures 6(a) and (c) the voltage is fixed to $V_0 = 13.22\,\mathrm{V}$ and a single localized structure is switched on by a triggering intensity pulse (state 1). Then, in panels (b) and (d) the voltage is increased to $V_0 = 13.30\,\mathrm{V}$ and the system is let to evolve. On each line, the successive panels correspond to the temporal evolution for reaching the final hexagonal state (state 2).

On the top line, we observe that new cells nucleate spontaneously over concentric rings around the first localized structure. Indeed, in the absence of any external perturbation, the only triggering signal for the nucleation of new localized structures is the slightly higher intensity of the rings around the first cell. When the voltage is slightly increased, the intensity on the rings increases and new cells are nucleated from the ring break-up, thus leading to a pattern with radial symmetry. Note that a similar behavior of spot nucleation over a ring has recently been reported for a planar Swift–Hohenberg equation [28]. When a small amplitude spatial noise is introduced in the simulation, the process of cell replication occurs instead in random space positions, which correspond to the small disturbances introduced by the noise. In this case, the

radial symmetry is completely destroyed, in agreement with the experimental observations (see figure 2). Indeed, in the experiment, due to the presence of spatial inhomogeneities in the liquid crystals, the structures nucleate in random space positions instead of following a regular path around the first cell.

5. Conclusions

In conclusion, we have shown that SLS exist outside the bistability range and that the transition from extended pattern to SLS is characterized by a dynamics of particle interaction and annihilation. The experimental and numerical observations are in qualitative and quantitative agreement.

Acknowledgments

We are grateful for the financial support by the ANR-07-BLAN-0246-03, *turbonde*. MGC acknowledges the financial support from the ring program ACT15 of Programa Bicentenario, FONDECYT project 1090045, and FONDAP grant 11980002.

References

[1] Newell A C 1985 *Solitons in Mathematics and Physics* (Philadelphia: Society for Industrial and Applied Mathematics)
[2] See, e.g. Cross M C and Hohenberg P C 1993 *Rev. Mod. Phys.* **65** 851
[3] O'Dell Th 1986 *Rep. Prog. Phys.* **49** 589
[4] Umbanhowar P B, Melo F and Swinney H L 1996 *Nature* **382** 793
[5] Clerc M G, Cordero P, Dunstan J, Huff K, Mujica N, Risso D and Varas G 2008 *Nat. Phys.* **4** 249
[6] Arbell H and Fineberg J 2000 *Phys. Rev. Lett.* **85** 756
[7] Dennin M, Ahlers G and Cannell D S 1996 *Science* **272** 388
[8] Astrov Y A and Logvin Y A 1997 *Phys. Rev. Lett.* **79** 2983
[9] Lee K-J, McCormick W D, Pearson J E and Swinney H L 1994 *Nature* **369** 215
[10] Tlidi M, Paul Mandel and Lefever R 1994 *Phys. Rev. Lett.* **73** 640
[11] Tlidi M, Taki M and Kolokolnikov T 2007 *Chaos* **17** 037101
[12] Taranenko V B, Staliunas K and Weiss C O 1998 *Phys. Rev. Lett.* **81** 2236
[13] Schäpers B, Feldmann M, Ackemann T and Lange W 2000 *Phys. Rev. Lett.* **85** 748
[14] Ramazza P L, Benkler E, Bortolozzo U, Boccaletti S, Ducci S and Arecchi F T 2002 *Phys. Rev.* E **65** 066204
[15] van Saarloos W and Hohenberg P C 1990 *Phys. Rev. Lett.* **64** 749
[16] Woods P D and Champneys A R 1999 *Physica* D **129** 147
[17] Hunt G W, Lord G J and Champneys A R 1999 *Comput. Methods Appl. Mech. Eng.* **170** 239
[18] Pomeau Y 1986 *Physica* D **23** 3
[19] Coullet P, Riera C and Tresser C 2000 *Phys. Rev. Lett.* **84** 3069
[20] Burke J and Knobloch E 2006 *Phys. Rev.* E **73** 056211
[21] Burke J and Knobloch E 2007 *Chaos* **17** 037102
[22] Clerc M G and Falcon C 2005 *Physica* A **356** 48
[23] Bortolozzo U, Clerc M G, Falcon C, Residori S and Rojas R 2006 *Phys. Rev. Lett.* **96** 214501
[24] Tissoni G *et al* 1999 *J. Opt. Soc. Am.* B **16** 2095
[25] Firth W J, Columbo L and Scroggie A J 2007 *Phys. Rev. Lett.* **99** 104503
[26] Dawes J H P 2008 *SIAM J. Appl. Dyn. Syst.* **7** 186

[27] Bortolozzo U, Clerc M G and Residori S 2008 *Phys. Rev.* E **78** 036214
[28] Lloyd D and Sandstede B 2009 *Nonlinearity* **22** 485
[29] Residori S 2005 *Phys. Rep.* **416** 201
[30] Clerc M G, Petrossian A and Residori S 2005 *Phys. Rev.* E **71** 015205
[31] Bortolozzo U and Residori S 2006 *Phys. Rev. Lett.* **96** 037801
[32] Tlidi M, Vladimirov A G and Mandel P 2002 *Phys. Rev. Lett.* **89** 233901
[33] Bortolozzo U, Pastur L, Ramazza P L, Tlidi M and Kozyreff G 2004 *Phys. Rev. Lett.* **93** 253901
[34] Residori S, Bortolozzo U and Ramazza P L 2006 *J. Low Temp. Phys.* **145** 277
[35] Coullet P, Toniolo C and Tresser C 2004 *Chaos* **14** 839
[36] Kolokolnikov T, Ward M J and Wei J 2009 *J. Nonlinear Sci.* **19** 1
[37] Kolokolnikov T and Tlidi M 2007 *Phys. Rev. Lett.* **98** 188303